# Supporting Information

# Portable multichannel immunoassay of Coxsackievirus A6 using a coordination-engineered iridium-doped ZIF-8 nanozyme

Fangming Zhu, Rongxiu Deng, Xue Liu, Guoliang Dai and Yuyang Zhou*

School of Chemistry and Life Sciences, Jiangsu Key Laboratory for Environmental Functional Materials, Suzhou University of Science and Technology, Suzhou, Jiangsu 215009, China

*Corresponding author

E-mail: zhouyuyang@mail.usts.edu.cn (Yuyang Zhou)

# Table of contents for supporting information

**Chemical Reagents and materials**

Zinc nitrate hexahydrate ($Zn(NO_3)_2•6H_2O$), 2-Methylimidazole (Hmim) and 2 aminobenzimidazole (2-amBzIM) were purchased from Aladdin (Shanghai, China). Dimethyl sulfoxide (DMSO), 2-ethoxyethanol, dichloromethane, methanol and acetonitrile were all brought from Jiangsu Qiangsheng Functional Chemistry Co., Ltd. Iridium(III) solvent complex (IrppyMeCN) was prepared by our laboratory and its synthesis was reported in our previous literature. 3,3',5,5'-Tetramethyl-benzyl (TMB) were purchased from Energy Chemical Inc. (Shanghai, China). 1-(3-dimethylaminopropyl)-3-ethylcarbodiimide hydrochloride (EDC) and N-hydroxy succinimide (NHS) were obtained from Bellwether Technology Co., Ltd. (Beijing, China). Test sheets was purchased from Baisi Biotechnology Co., Ltd (Hangzhou, China). N-(2-hydroxyethyl)piperazine-N'-2-ethanesulfonic acid (HEPES) was purchased from Macklin Biochemical Technology Co., Ltd. (Shanghai, China).

**Apparatus**

The morphology and size of the obtained products were studied using a Regulus 8100 scanning electron microscope with an operating voltage of 20 kV. The powder X ray diffraction (PXRD) patterns were obtained using a Bruker D8 Advance X-ray diffractometer with Cu Kα radiation source (40 kV, 40 mA) over a 2θ range of 5-50°. Fourier-transform infrared (FT-IR) spectra were recorded using a JASCO FT/IR-430 spectrometer in the wavenumber range of 500-4000 cm-1. TOF mass spectrum were measured on Bruker ultrafleXtreme. X-ray photoelectron spectroscopic (XPS) analysis was performed on Thermo Kalpha Xray photoelectron spectrometer (Thermo Fisher Scientific, America). Uv-vis spectrophotometer (TU-1950, Beijing Purkinje General Instrument Co., LTD., Beijing, China) was used to measure UV-VIS and PL spectra. CV data were collected by CHI660E workstation (Chenhua Instrument Co., LTD., Shanghai, China). A photomultiplier tube (model: R9880U-20, Hamatsu, Japan, spectral response range :230-920 nm) was mounted on an MPI-EII ECL detector (Xi 'an Ruima Electronics, China) to measure the CV and ECL photocurrent signals. The combination of an electrochemical workstation (CHI660E) and a fiber optic spectrometer (Suzhou Puzhu Optoelectronics Technology Co., LTD., model: PSVNS460_4G) can be used to record the spool ECL spectra of the metal complex

The study protocol was approved by the ethics review board of Suzhou University of Science and Technology (No. USTS2024002). We have obtained written informed consent from all study participants. All of the procedures were performed in accordance with the Declaration of Helsinki and relevant policies in China

All viral samples used in the experiments were subjected to inactivation treatment.

**DFT calculation details**

In the present work, the first-principle calculations were applied using the Vienna ab initio software package (VASP) with the projector augmented wave method.[1-3] Meanwhile, the generalized gradient approximation (GGA) within the Perdew-Burke-Ernzerhof (PBE) was adopted to compute the electron exchange-correlation energy.[4] The structure was relaxed via a cutoff energy of 500 eV. The atomic position, cell volume, as well as cell shape was fully optimized until the forces lower than 0.01 eV $Å^{-1}$. The spin-polarization was taken into account in all calculations. The structure of ZIF-8 was assumed to form by the tetrahedral coordination of zinc ions and imidazolate ligands. The cluster containing four zinc ions is selected as the basic construction unit for ensuring the accuracy of calculation. The 20 Å vacuum layer was normally added to the surface to eliminate the artificial interactions between periodic images, and the (3 × 3 × 1) grid was employed for K−space sampling during all the calculations. All possible initial geometries were considered and the optimized ones with the lowest energy were reported. The adsorption energy (*E*ad) was calculated according to

$$E\text{ad} = E\text{gas−surf} - (E\text{surf} + E\text{gas})$$

where *E*gas, *E*surf, and *E*gas−surf represent the energies of the gas molecule, the clean Zif-8 and the corresponding adsorbed gas molecule on Zif-8 surface, respectively.

**Microscopic characterization images of Ir-ZIF-8-COOH**

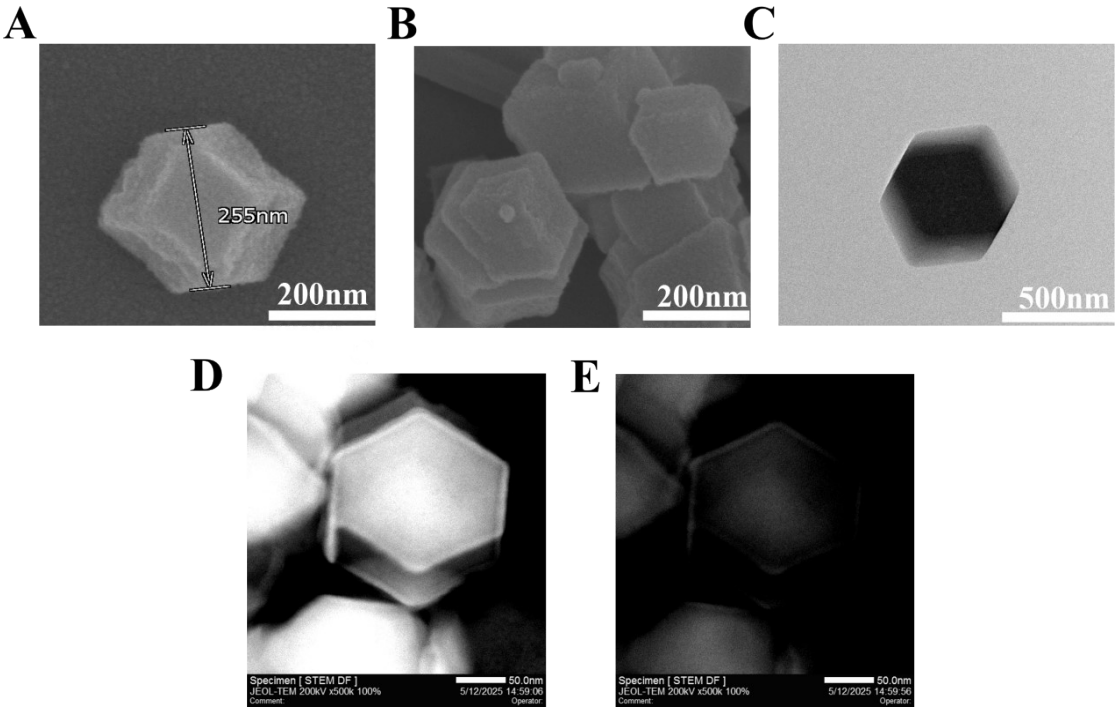


Fig. S1. (A-B) SEM image of Ir-ZIF -8-COOH. (C) TEM image of Ir-ZIF-8-COOH (D) Magnified HAADF STEM of C/N/O/Zn/Ir and (E) Ir/Zn

## EDS analysis of as-prepared MOF-based nanocomposite Ir-ZIF-8-COOH

Acquisition 2474

| Element | At. No. | Line s. | Netto | Mass [%] | Mass Norm. [%] | Atom [%] | abs. error [%] (1 sigma) | abs. error [%] (2 sigma) | abs. error [%] (3 sigma) | rel. error [%] (1 sigma) | rel. error [%] (2 sigma) | rel. error [%] (3 sigma) |
|---|---|---|---|---|---|---|---|---|---|---|---|---|
| Nitrogen | 7 | K-Serie | 7883 | 31.70 | 31.70 | 65.74 | 1.04 | 2.08 | 3.12 | 3.28 | 6.57 | 9.85 |
| Oxygen | 8 | K-Serie | 2564 | 5.20 | 5.20 | 9.45 | 0.21 | 0.42 | 0.64 | 4.07 | 8.14 | 12.22 |
| Zinc | 30 | K-Serie | 28803 | 52.10 | 52.10 | 23.15 | 1.62 | 3.24 | 4.87 | 3.11 | 6.23 | 9.34 |
| Iridium | 77 | L-Serie | 3728 | 10.99 | 10.99 | 1.66 | 1.15 | 2.30 | 3.45 | 10.47 | 20.94 | 31.41 |
| | | | **Sum** | **100.00** | **100.00** | **100.00** | | | | | | |

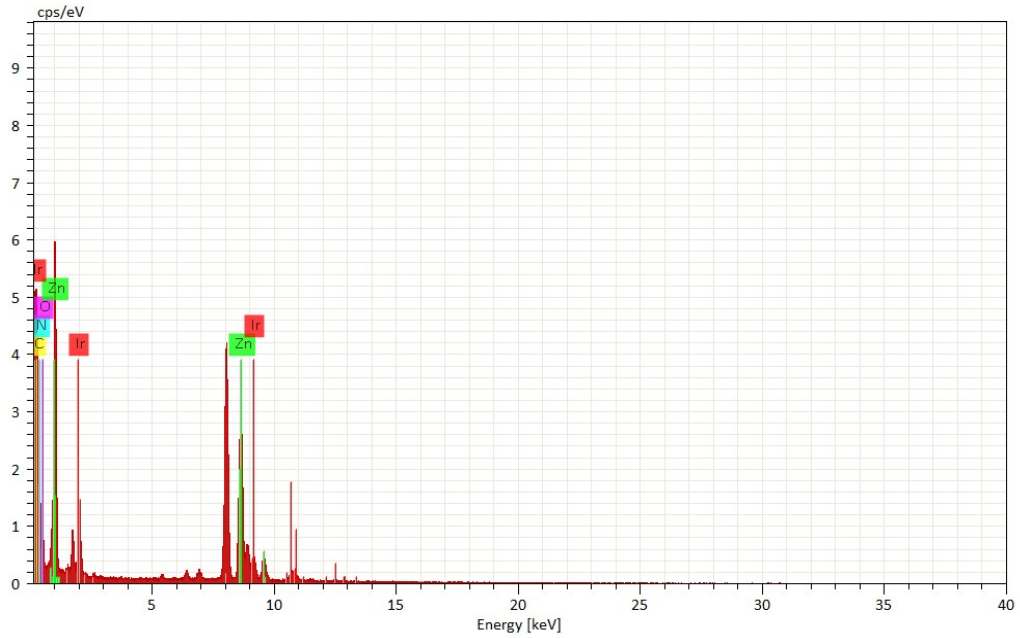


Fig. S2. EDS analysis of as-prepared MOF-based nanocomposite Ir-ZIF-8-COOH

**FI-IR spectra of as prepared ZIF-8 and Ir-ZIF-8.**

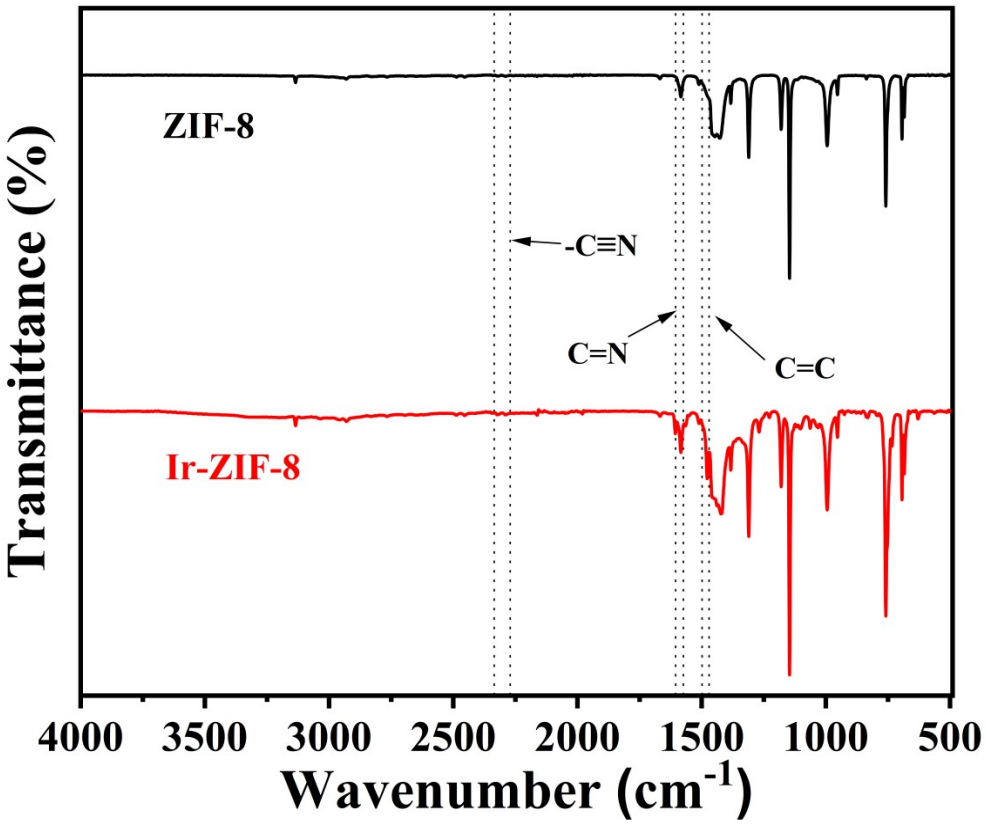


Fig. S3. FI-IR spectra of as prepared ZIF-8 and Ir-ZIF-8.

**The UV spectrum of the Ir-ZIF-8-COOH+$H_2O_2$+TMB and $H_2O_2$+TMB.**

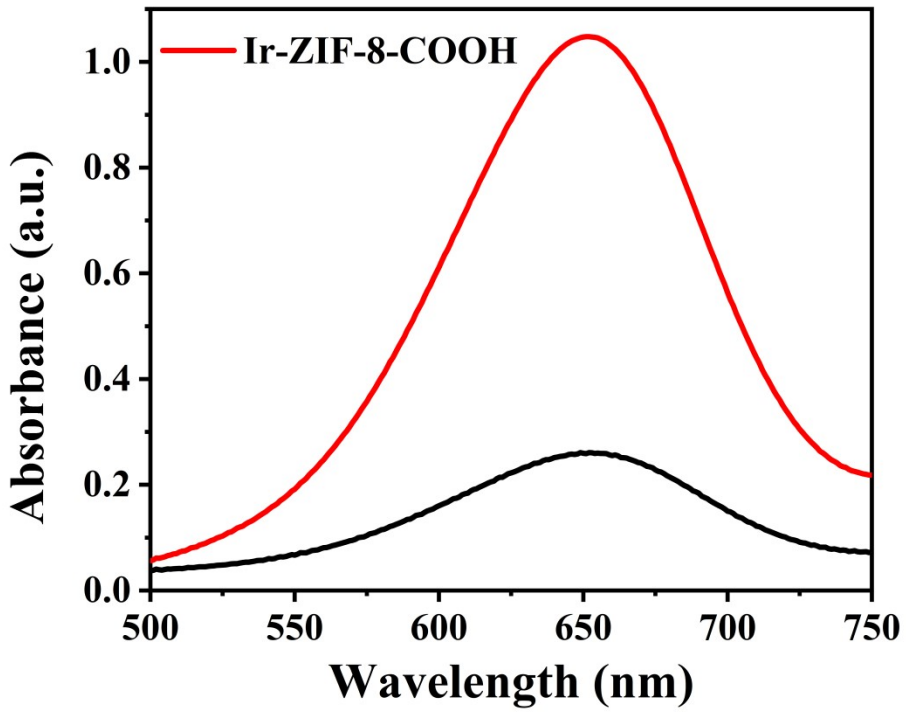


Fig. S4. The UV spectrum of the Ir-ZIF-8-COOH+$H_2O_2$+TMB and $H_2O_2$+TMB.

**Theoretical models of the ZIF-8 and Ir-ZIF-8.**

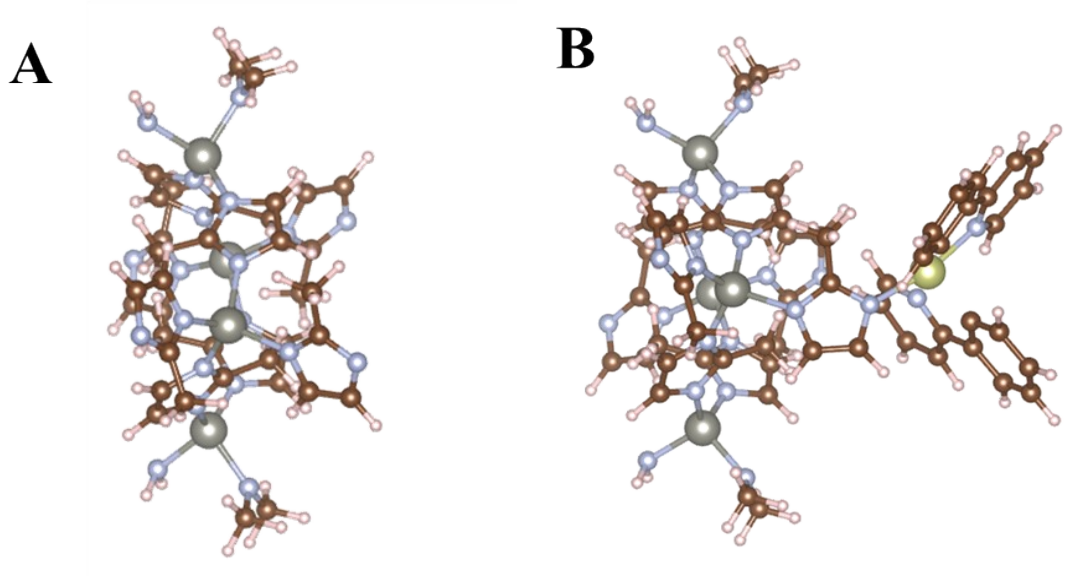


Fig. S5. Theoretical models of the ZIF-8 and Ir-ZIF-8.

**The DFT simulation calculation of the reaction between the Ir-ZIF-8 and $H_2O_2$.**

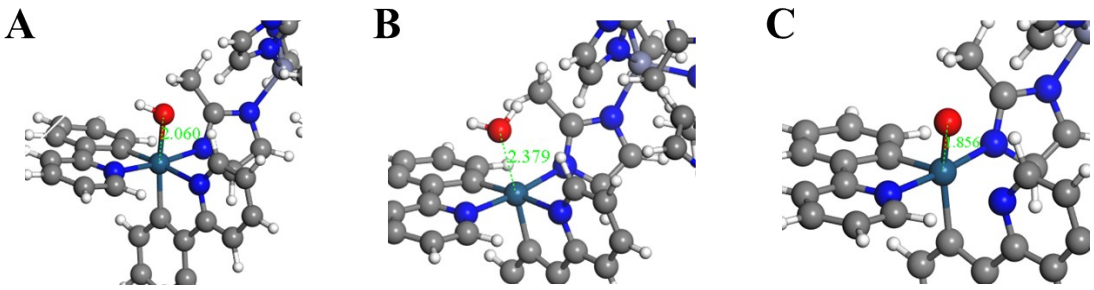


Fig. S6. The DFT simulation calculation of the reaction between the Ir-ZIF-8 and $H_2O_2$.

**The PL intensity of Ir-ZIF-8 and Ir-ZIF-8 + $H_2O_2$**

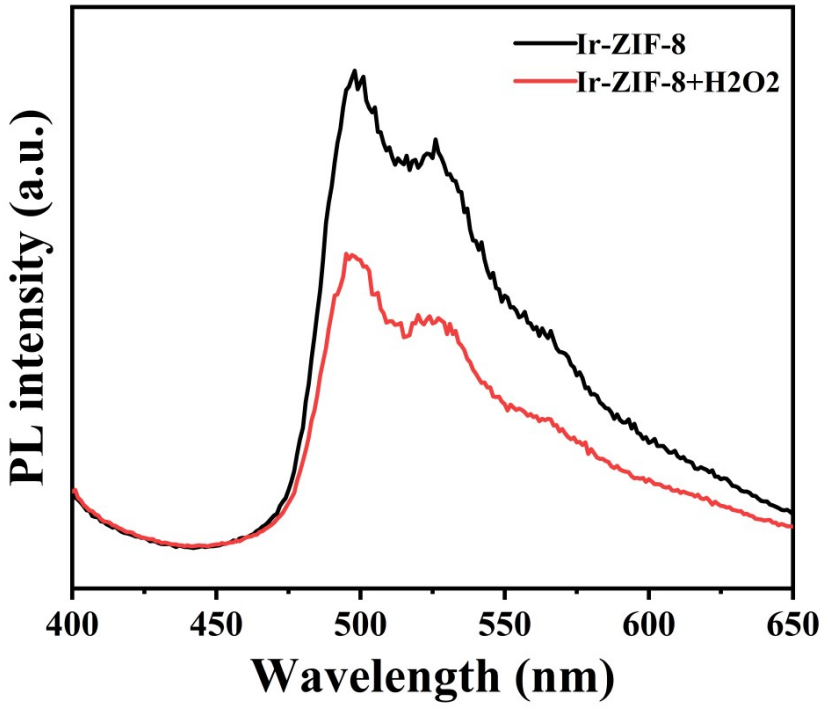


Fig. S7. The PL intensity of Ir-ZIF-8 and Ir-ZIF-8 + $H_2O_2$.

**The EPR spectrum of the Ir-ZIF-8-COOH and IrppyMeCN.**

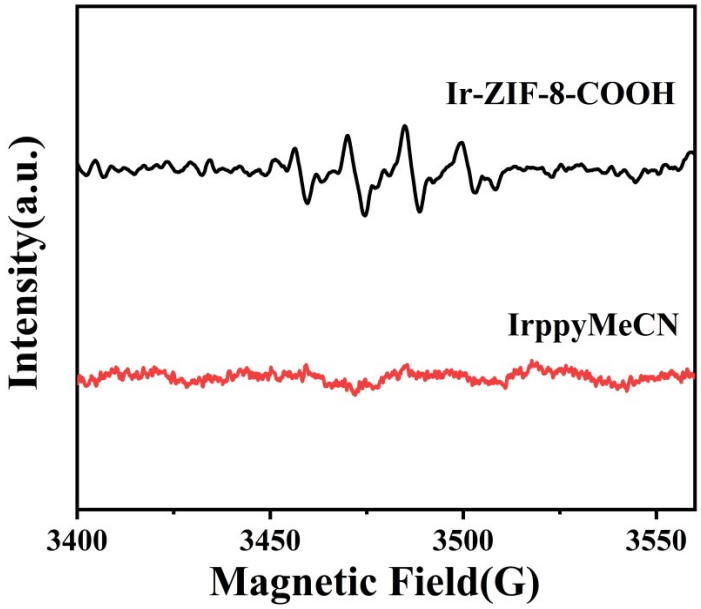


Fig. S8. The EPR spectrum of the Ir-ZIF-8-COOH and IrppyMeCN.

**The Optimization of different concentration of $H_2O_2$ (0.5-5mM) in ECL mode.**

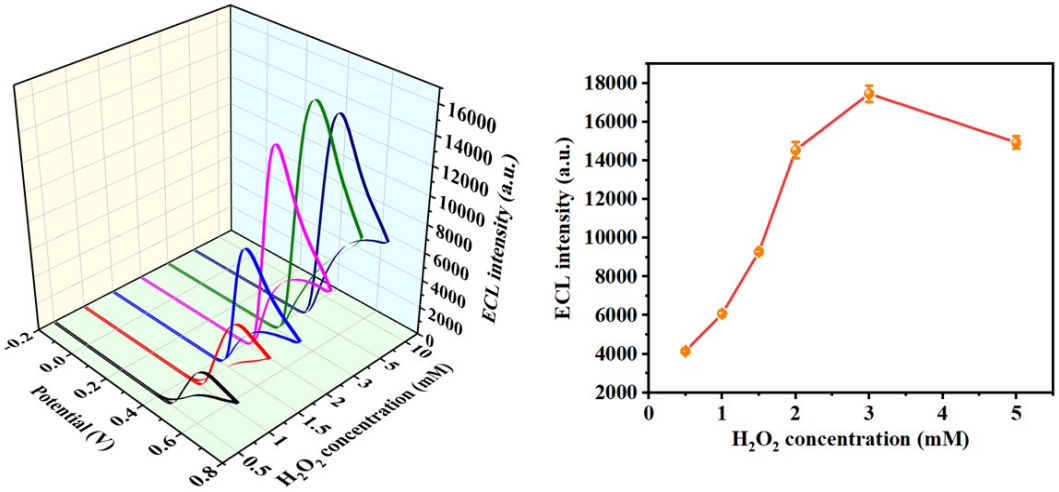


Fig. S9. The Optimization of different concentrations of $H_2O_2$ (0.5-5mM) in ECL mode.

**The Optimization of different concentrations of luminol (0.01-0.5mM) in ECL mode**

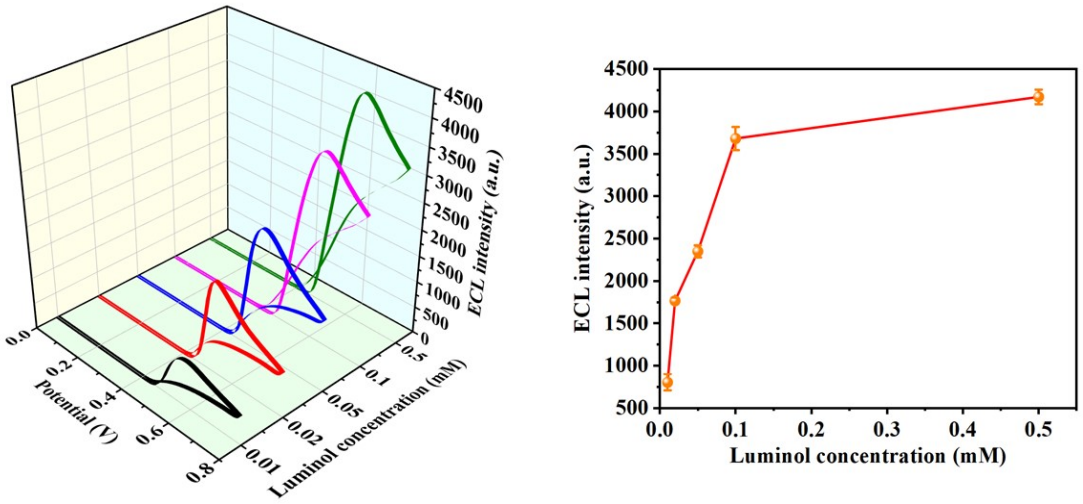


Fig. S10. (A) The Optimization of different concentrations of luminol (0.01-0.5mM) in ECL mode

**The Optimization of temperature and pH in ECL mode.**

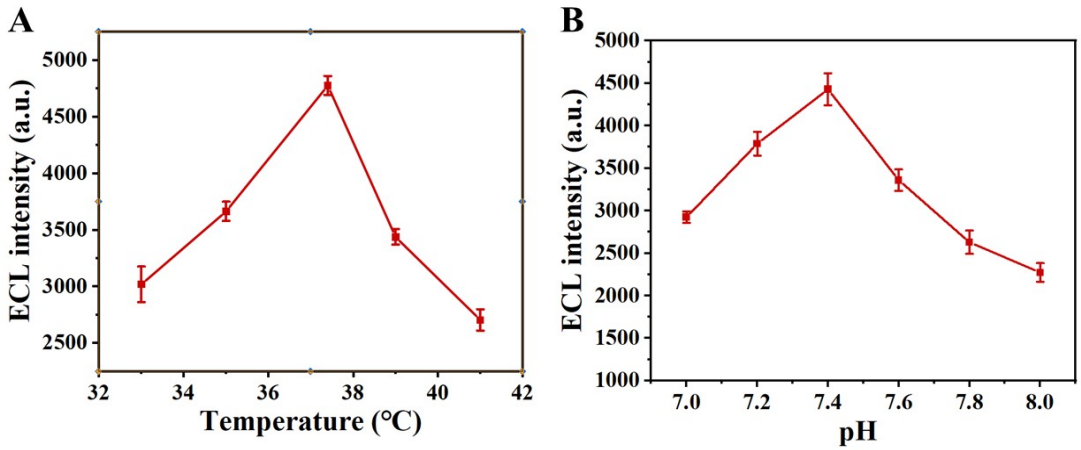


Fig. S11. The Optimization of temperature (A) and pH (B) in ECL mode.

**ECL intensity of luminol, $H_2O_2$+ luminol, Ir-ZIF-8-COOH and Ir-ZIF-8-COOH+ $H_2O_2$+luminol**

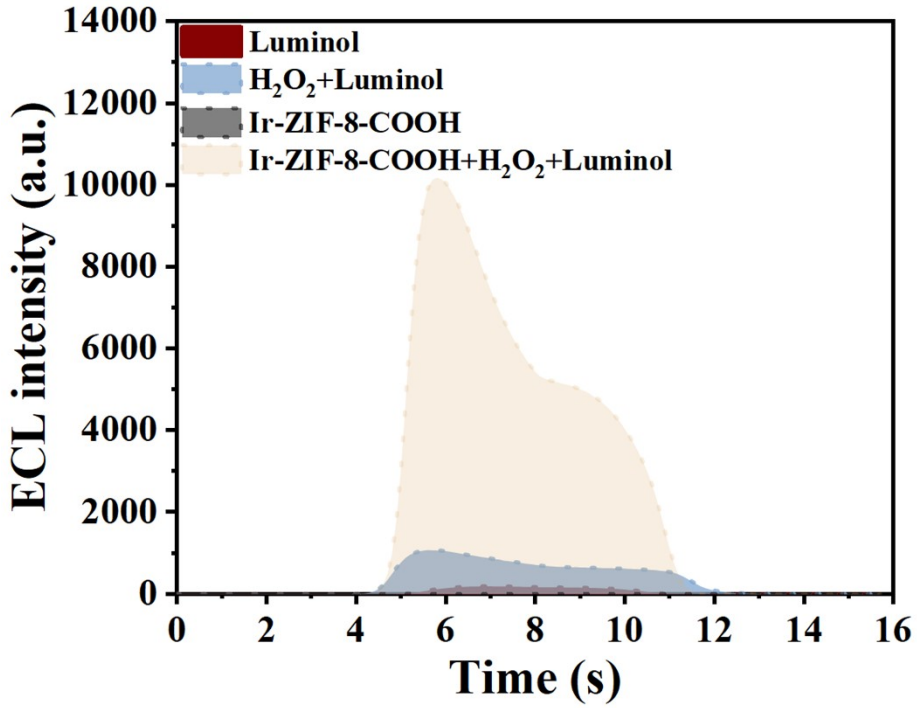


Fig. S12. ECL intensity of luminol, $H_2O_2$+ luminol, Ir-ZIF-8-COOH and Ir-ZIF-8-COOH+ $H_2O_2$+luminol

**The Optimization of pH in colorimetric mode**

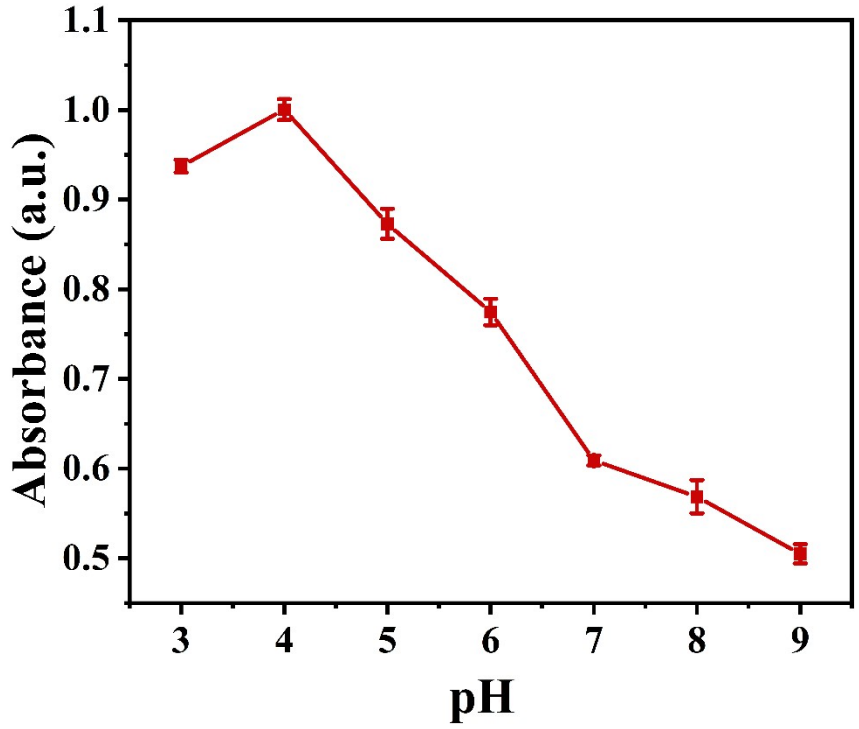


Fig. S13. The Optimization of pH in colorimetric mode

**The curve of CVA6 RGB colorimetric mediated sensor using the (R+B)/2G and (G+B)/2R formula**

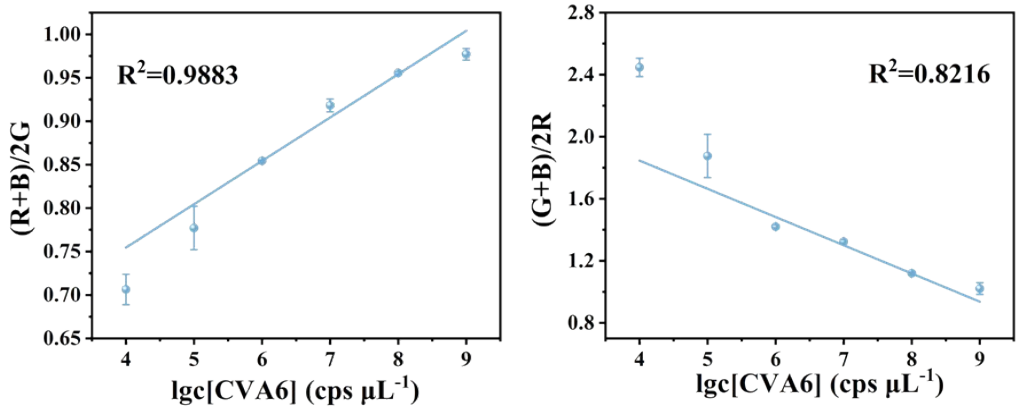


Fig. S14. The curve of CVA6 RGB colorimetric mediated sensor using the (R+B)/2G and (G+B)/2R formula.

**Optimization of temperature and pH in PL mode**

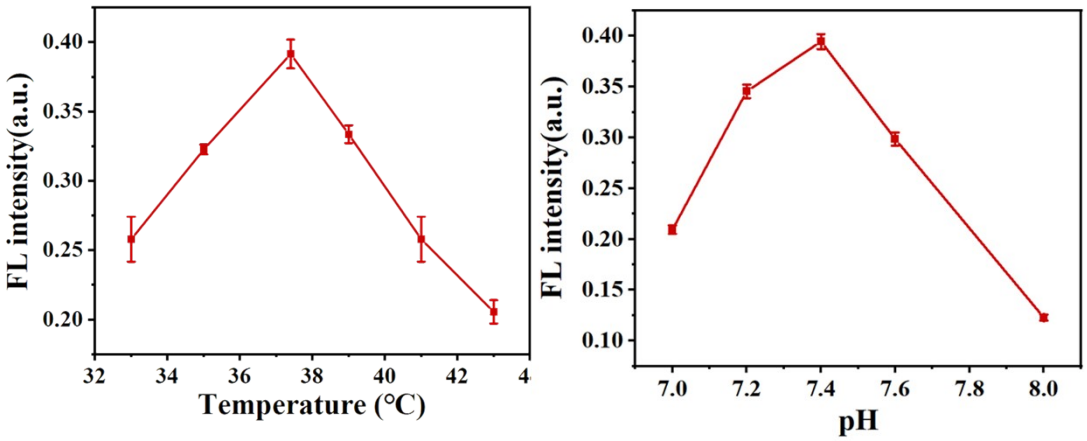


Fig. S15. Optimization of temperature and pH in PL mode

**PL curve of the proposed sensor when scanning continuously for 11 cycles after incubation with $10^5$ cps/µL CVA6 in PL mode**

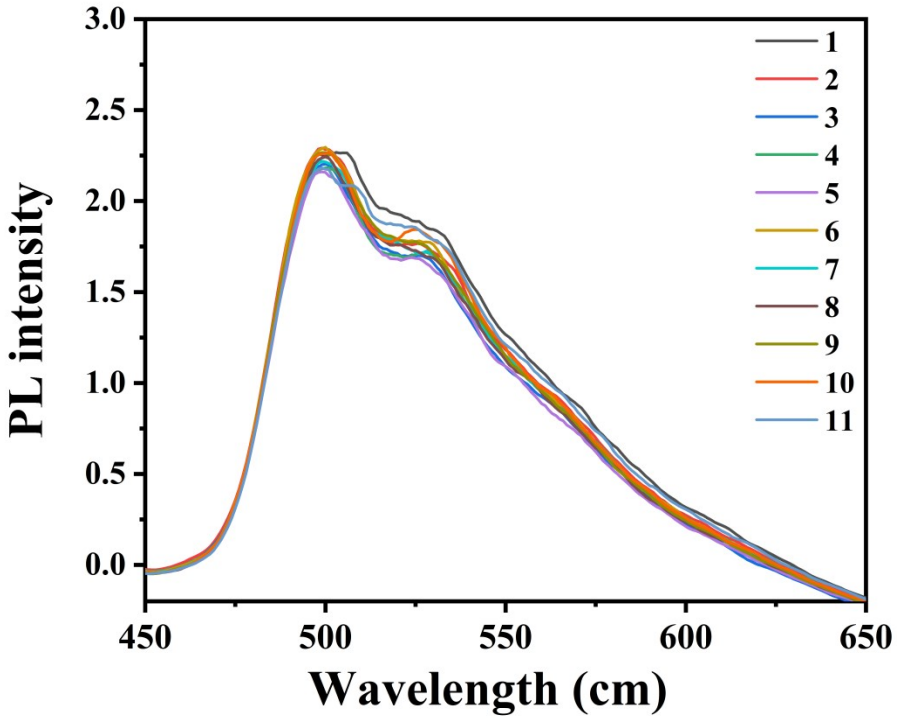


Fig. S16. PL curve of the proposed sensor when scanning continuously for 11 cycles after incubation with $10^5$ cps/µL CVA6 in PL mode.

**Table S1. Comparison of Km and Vmax between Ir-ZIF-8-COOH with other catalysts**

| Catalyst | Substrate | Km (mM) | Vmax ($10^{-7}$ M $s^{-1}$) | Ref |
|---|---|---|---|---|
| HPR | TMB | 0.434 | 10 | [5] |
| | $H_2O_2$ | 3.7 | 8.71 | |
| $Fe_3O_4$ | TMB | 0.098 | 3.44 | [5] |
| | $H_2O_2$ | 154 | 9.78 | |
| [Ir(III)/GO] | TMB | 0.1514 | 7.1471 | [6] |
| | $H_2O_2$ | 0.3486 | 8.1431 | |
| Fe/Mn-SNC | TMB | 0.17 | 4.746 | [7] |
| | $H_2O_2$ | 8.88 | 9.456 | |
| ZIF-8 | TMB | 0.224 | 10.66 | [8] |
| | $H_2O_2$ | 40.16 | 12.15 | |
| Ir-ZIF-8-COOH | TMB | 0.0962 | 1.4650 | This |
| | $H_2O_2$ | 7.5453 | 23.946 | work |

## Reference


1. G. Kresse and J. Furthmüller, *Physical Review B*, 1996, **54**, 11169-11186.
2. G. Kresse and J. Furthmüller, *Computational Materials Science*, 1996, **6**, 15-50.
3. P. E. Blöchl, *Physical Review B*, 1994, **50**, 17953-17979.
4. J. P. Perdew, K. Burke and M. Ernzerhof, *Phys. Rev. Lett.*, 1996, **77**, 3865-3868.
5. L. Gao, J. Zhuang, L. Nie, J. Zhang, Y. Zhang, N. Gu, T. Wang, J. Feng, D. Yang, S. Perrett and X. Yan, *Nature Nanotechnology*, 2007, **2**, 577-583.
6. L. Wang, W.-J. Zeng, X. Yang, R. Yuan, W.-B. Liang and Y. Zhuo, *Anal. Chem.*, 2023, **95**, 13897-13903.
7. C. Jiang, M. Sun, Y. Wang, C. Dong, Y. Yu, G. Wang, Y. Lu and Z. Chen, *Adv. Funct. Mater.*, 2025, **n/a**, 2424599.
8. B. Xu, H. Wang, W. Wang, L. Gao, S. Li, X. Pan, H. Wang, H. Yang, X. Meng, Q. Wu, L. Zheng, S. Chen, X. Shi, K. Fan, X. Yan and H. Liu, *Angew. Chem. Int. Ed.*, 2019, **58**, 4911-4916.